2014

Enhancing the Insulation of Wide-Range Spectrum in the PVA/N Thin Film by Doping ZnO Nanowires

Yu-Chen Lin

Ching-Hsiang Vhen

Liang-Yih CHen

Shih-Chieh Hsu

Shizhi Qian
Old Dominion University, sqian@odu.edu

Repository Citation

Original Publication Citation

PAPER

Enhancing the insulation of wide-range spectrum in the PVA/N thin film by doping ZnO nanowires

Yu-Chen Lin,[a] Ching-Hsiang Chen,[b] Liang-Yih Chen,[c] Shih-Chieh Hsu*[de] and Shizhi Qian[f]

In this study, polyvinyl alcohol/nitrogen (PVA/N) hybrid thin films doped with sharp-sword ZnO nanowires with insulating effect and wide-range spectrum are demonstrated for the first time. PVA/N doped ZnO nanocomposites were developed by blending PVA and N-doped ZnO nanowires in water at room temperature. Measurements from the field emission scanning electron microscopy (FE-SEM), X-ray diffraction (XRD), Raman, and photoluminescence emission (PL) spectra of the products show that nitrogen is successfully doped into the ZnO wurtzite crystal lattice. In addition, the refractive index of PVA/N doped ZnO hybrid thin films can be controlled by varying the doped ZnO nanowires under different NH_3 concentrations. It is believed that PVA/N doped ZnO hybrid thin films are a suitable candidate for emerging applications like heat-shielding coatings on smart windows.

1. Introduction

Polymer matrix nanocomposites with inorganic nanofillers, particularly with metal oxides, have drawn significant attention due to their potential applications in optical products.[1–3] Because of their unique optical, electrical, and mechanical properties, polymer matrixes and metal oxides can be synthesized together as novel materials used in many potential applications.[4,5] For example, in the smart window application, the heat shielding films are able to control the sunlight energy spectrum because the visible light needs to be transmitted while the near-infrared light should be cut for thermal insulation, producing the energy-saving effect. Recently, the coatings with low emissivity heat shielding have also attracted significant attention because polymer nanocomposites with metal oxide nanofiller can modify the optical, thermal, and mechanical properties.[6–8]

Polyvinyl alcohol (PVA) has several advantages such as easy synthesis, non-toxicity, water-solubility, transparency, good environmental stability, thermal stability, and film-forming ability.[9] It is also a promising material for the development of optical, pharmaceutical, biomedical and membrane applications.[10] Furthermore, polymer/metal oxide nanocomposites can be formed *via* hydrogen bonding between the –OH groups of PVA and the functional groups of metal oxides.[11]

Among all metal oxide materials, zinc oxide (ZnO) is an n-type semiconductor material with a wide band gap ($E_g = 3.34$ eV), although this definition is still under debate.[12] It has high exciton binding energy (60 meV) and it has attracted a significant interest over the past decade because of the presence of native defects related to oxygen vacancies and shallow zinc interstitials, both of which act as donors.[13–16] Some investigations report that ZnO can not only act as donors, but also as acceptors.[17,18] It also shows some beneficial properties, including good transparency, high electron mobility, and strong luminescence.[13–16] Therefore, ZnO is typically adopted as transparent films in several emerging applications, including the energy-saving and heat shielding smart window, thin-film transistors, light-emitting diodes,[19–21] solar cells,[22,23] and biomedical applications.[24] To further improve its performance in optoelectronic applications, ZnO based nanomaterials have been developed by doping group I and V elements.[25–32] Many experimental results show that substituting O sites of ZnO can modulate its electrical and optical properties. Among various dopant elements, nitrogen is the most promising candidate because of its smallest ionization energy and its atomic radius, which is similar to the one of oxygen.[33,34]

The optical properties of pure PVA polymer films show no remarkable absorption bands in the range of UV-Vis and easily generate photodegradation when they are exposed to UV light.[35] Several methods have been applied by combining ZnO derivatives with the PVA during film-forming. For example, Augustine *et al.*[6]

[a]*Department of Photovoltaic Materials Equipment, Precision Machinery Research & Development Center, 569, Sec II, Po-Ai Rd., Chiayi City 60060, Taiwan*

[b]*Graduate Institute of Applied Science and Technology, National Taiwan University of Science & Technology, Taipei, Taiwan*

[c]*Department of Chemical Engineering, National Taiwan University of Science and Technology, 43, Section 4, Keelung Road, Taipei, 106, Taiwan*

[d]*Department of Chemical and Materials Engineering, Tamkang University, Tamshui, New Taipei City, 25137, Taiwan. E-mail: roysos@mail.tku.edu.tw; Fax: +886-26209887; Tel: +886-26215656 ext. 2032*

[e]*Energy and Opto-Electronic Materials Research Center, Tamkang University, Tamshui, New Taipei City, 25137, Taiwan*

[f]*Institute of Micro/Nanotechnology, Old Dominion University, Norfolk, VA 23529, USA*

introduced oleic acid containing groups onto the surfaces of ZnO nanorods embedded in PVA matrix to prepare the highly transparent nanocomposite films. Moreover, Tan et al.[36] reported that the performance of PVA/ZnO nanorods redox sensors is enhanced because of the properties of ZnO, which effectively facilitates the electron transfer and provides better stability and stronger signal. Subsequently, Roy et al.[37] reported the relaxation, electronic transportation, and conduction mechanism of PVA/ZnO nanocomposites by a solution casting technique, which is influenced by the applied frequencies. However, these studies[35–37] pointed out that the PVA/N thin films doped ZnO were only able to insulate UV light. The limitation of light insulation hinders the applications in the use of heat shielding materials. Here, the "Optical insulation" is defined as an ability to partially block the light from UV to IR. Because the PVA/N doped ZnO thin film can effectively block the sun light outside, it also has the function of heat insulation. The combined features of optical and heat insulations enable the hybrid film to become a suitable candidate for energy-saving applications such as heat-shielding coatings on smart windows.

In order to achieve a wide-range spectrum insulation, we propose a simple and effective method to prepare PVA hybrid thin films with sharp-sword ZnO nanocomposites by controlling N species in the ZnO nanowires. We found that doping N into the entire system to form the sharp-sword ZnO nanowires can insulate the wide-range spectrum, especially the IR light, because there are defects in the ZnO nanowires. Our technique of PVA/N doped with sharp-sword ZnO nanowires is capable of insulating the wide-range spectrum instead of only the UV spectrum reported in previous studies. The structure, morphology, and optical properties of N-doped ZnO nanowires will be characterized by using XRD, PL, and Raman scattering. The correlations between the experimental conditions and the performance of the PVA/N doped ZnO hybrid thin films will be investigated and discussed in detail by the spectroscopic technique.

2. Experimental

2.1. Materials

Polyvinyl alcohol (PVA, 98–99% hydrolyzed, MW 13 000–23 000) and polyethyleneimine (PEI, MW 800) were purchased from Aldrich. Zinc acetate dihydrate ($Zn(OAc)_2 \cdot 2H_2O$) and hexamethylenetetramine [$(CH_2)_6N_4$] were purchased from Merck. Indium tin oxide (ITO) glass substrates, whose content is $Sn_2O_3 : In_2O_3 = 1 : 9$, were purchased from Lumtec. Deionized (DI) water with resistivity of 1 MΩ cm was prepared by a deionized water machine (model: RDI-20) produced by Lotuntech.

2.2. Preparation of the N-doped ZnO nanowires

The N-doped ZnO nanowires were synthesized by the hydrothermal method. First, $Zn(OAc)_2 \cdot 2H_2O$ (25 mM), $(CH_2)_6N_4$ (25 mM) and PEI molecules (5 mM) were dissolved individually in DI water to form a 40 mL solution. ITO glass substrates were sequentially immersed into the detergent, DI-water, ethanol,

and 1-propanol and washed by ultrasonic bath. After washing, the ITO glass substrates were blown by N_2 gas for drying. We stirred the mixture at room temperature for 1 h to form a homogeneous solution and then placed it into the Teflon-lined steel autoclave for 90 °C for 24 h. The line-type growth began to form ZnO nanowires onto the ITO substrate. After growth process, the samples were rinsed with DI water to remove any residual salt or amino complex. Subsequently, the samples were dried under vacuum for 12 h at 60 °C to obtain the pristine ZnO (referred to as sample S1). Finally, the samples were annealed at 400 °C for 2 h in ambient air. We obtained the doped S2 and S3 samples using NH_3 to adjust the solution pH to 9 and 11, respectively.

2.3. Preparation of the PVA/N doped ZnO thin film

The PVA/N doped ZnO nanocomposite was prepared by ultrasonically dispersing the N-doped ZnO nanowires into the PVA solution (PVA/N doped ZnO: 1000 mg/20 mg, DI water: 15 mL), and the mixture was stirred and heated at 100 °C for 1 h. Then, we used the spin-coating technique to form a PVA/N doped ZnO thin film, which has 2 wt% of N-doped ZnO nanowires. The thickness of the films was controlled by the coating times (5 layers) and the speed of the spin-coating unit (3000 rpm). Finally, the films, labeled as PVA, PVA/S1, PVA/S2, and PVA/S3, were heated to 40 °C for 10 min.

2.4. Equipments and measurements

The morphology was analyzed by field emission scanning electron microscopy of Hitachi S-5000 system (Hitachi, Japan). X-ray diffraction patterns were characterized by a Rigaku X-ray diffractometer (model-D/Max-2B, Cu Kα radiation at a scan rate of 1° min^{-1} from 20°–75°, 30 kV). The RAMaker system (Protrustech Corporation Limited), which can measure 532 nm diode pumped solid state (DPSS) laser excited Raman spectra and 325 nm He–Cd laser PL spectra, is equipped with one Andor iDus TE cooled CCD of 1024 × 128 pixels. The ellipsometry data was collected by Elli-SE (Ellipso Technology Company) to obtain the n and k values of the PVA/N doped ZnO nanocomposite on glass films.

3. Results and discussion

In Fig. 1, the morphologies of the as-grown pristine ZnO and N-doped ZnO nanowires were observed by FE-SEM. As shown in Fig. 1a, the pristine ZnO nanowires (S1) shape like irregular columns with diameters of approximately 300–400 nm. However, the diameter of the N-doped ZnO nanowires (S2) was about 100–200 nm with a length of about 2 μm. The N-doped ZnO nanowires (S2) possess high density and evenly grow along the axis. The results indicated that NH_3 could restrain the lateral growth of ZnO (Fig. 1b).[44] When pH is increased to 11, the N-doped ZnO nanowires adopt a sharp-pointed shape with diameters of 400–900 nm (Fig. 1c). These morphologies were similar to those observed on the as-grown phosphorus-doped p-type ZnO nanowires by the hydrothermal method.[26]
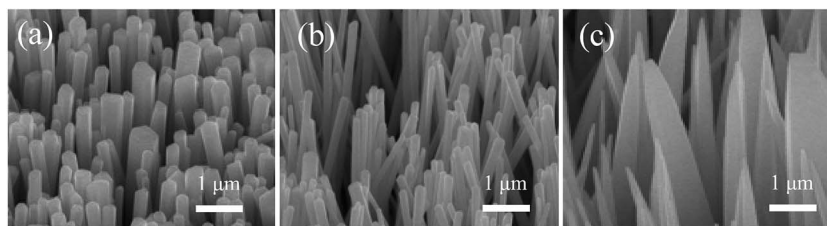
Fig. 1   FE-SEM images of the pristine ZnO and N-doped ZnO nanowires prepared in (a) S1, (b) S2, and (c) S3.

The properties of the nitrogen doped into ZnO crystal lattices prepared by the hydrothermal method were further investigated. The XRD measurements of the pristine ZnO and N-doped ZnO nanowires prepared under the alkaline environment are shown in Fig. 2. A magnification of the (002) diffraction peaks was observed (inset in Fig. 2). The diffraction peak at 34.4° observed in the pristine ZnO (S1) can be attributed to the ZnO wurtzite crystal structure, which is a preferential crystal orientation along the *c*-axis (Fig. 2a).[26,38] In the XRD spectrum of N-doped ZnO nanowires (S2 and S3), diffraction still peaks at 34.4° (Fig. 2b and c). For S1, S2 and S3, the full-width at half maximum (FWHM) of the (002) diffraction peak were 0.31°, 0.33°, and 0.40°, respectively. These results reveal that the crystallinity of ZnO nanowires slightly decreased with the doped N ions. This may be because of the fact that the preferential adsorption of NH_3 on crystal lattice causes the N ions to substitute the Zn sites to form complex defects,[26,38,39] a situation that is similar to the Ag–N doped p type ZnO films prepared by sol–gel method.[40]

Fig. 3 depicts the Raman spectra of the samples S1, S2, and S3. There are wurtzite ZnO structures in the undoped ZnO nanowires, including 332, 383, 438, 584 and 1158 cm^{-1}. The corresponding models of molecular movement are 2-E_2 (M), A_1 (TO), E_2 (high frequency), E_1 (LO) modes, and C–O bonds.[41–44] In the Raman spectrum of S2, spectral peaks at approximately 278, 511, 584 and 645 cm^{-1} were observed (Fig. 3b). These peaks indicate that several modes were formed because of the nitrogen-related local vibrational modes of the N-doped ZnO by the NH_3 treatment.[44–47] When the pH of the solution increases, the spectral peaks of the S3 become more obvious than those of

Fig. 2   XRD spectra of the pristine ZnO and N doped ZnO nanowires prepared in (a) S1, (b) S2, and (c) S3. Inset: the magnification of the (002) diffraction peaks.
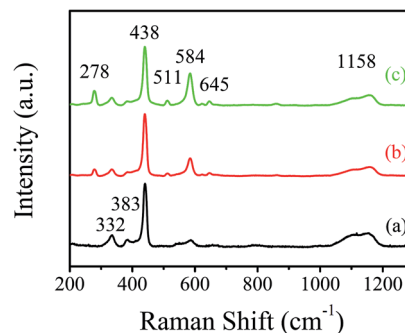

Fig. 3   Raman spectra of the pristine ZnO and N-doped ZnO nanowires prepared in (a) S1, (b) S2, and (c) S3.

the samples S1 and S2 (Fig. 3c). This finding may be attributed to the increase in nitrogen content in the N-doped ZnO nanowires, which formed the defects by N incorporation. The results were consistent with the XRD analysis (Fig. 2) and similar to the stable p-type ZnO film, which was fabricated by radio frequency sputter deposition and ion beam sputter deposition on Si and quartz glass substrates by nitrogen doping.[48,49]

Fig. 4 shows the PL spectra, excited by a 325 nm He–Cd laser, of the pristine ZnO and N-doped ZnO nanowires at various pH values at room temperature. The peak of ultraviolet emission at about 382 nm of the pristine ZnO nanowires could be identified. The peak appears because the near band-edge excitonic emission (NBE) of ZnO is generated by the recombination of the free excitons *via* an exciton collision process (inset in Fig. 4a).[26,50–52] In regards to N-doped ZnO nanowire, the near band-edge emission will lead to a blue-shift from 382 to 379 nm. If we increase the pH to produce the N-doped ZnO, the emission intensity of the ultraviolet area decreases (inset in Fig. 4b and c). These results indicated that the shift of the peak in the UV region tends toward high energy, probably because the O sites are replaced by N in the ZnO crystal lattices.[26,52,53]

In addition, the intensity of visible emission related to the defects in the pristine ZnO nanowires was weak (Fig. 4a). The intensity of orange emission of N-doped ZnO nanowires at about 607 and 624 nm become stronger with the increase of pH values (Fig. 4b and c). The orange emission is related to the intrinsic defects that are formed with N incorporated with the ZnO, such as oxygen vacancy or zinc intrinsic.[26,52–55] The behavior is consistent with the analyses of XRD and Raman spectra. The wavelength of PL emission is observed to be higher in the region of orange emission than the results reported in the
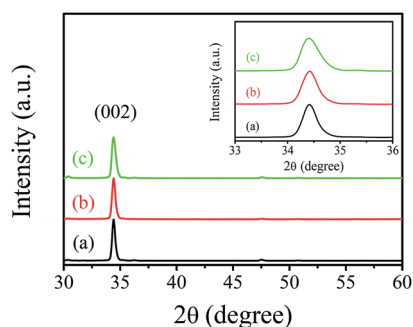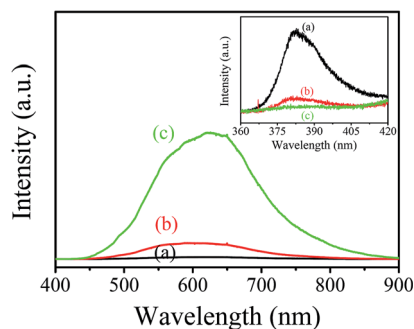
Fig. 4 PL spectra of the pristine ZnO and N-doped ZnO nanowires prepared in (a) S1, (b) S2, and (c) S3. Inset: the magnification of the ultraviolet emission region.
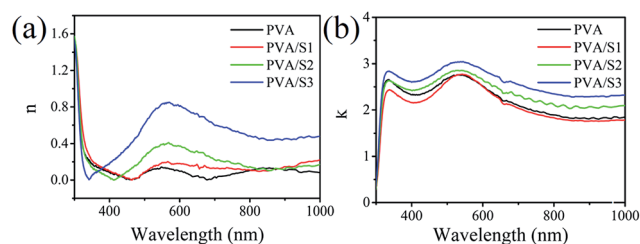

Fig. 5 (a) Refractive indices and (b) extinction coefficients spectrum for the PVA, PVA/pristine ZnO and PVA/N doped ZnO hybrid nano-composite films.
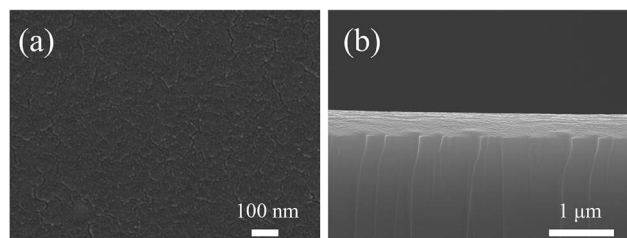

Fig. 6 FE-SEM images of the PVA/N doped ZnO (S3) thin films prepared (a) planar and (b) cross-section.

literature,[4,13] in which Cu is doped into ZnO nanoparticle sheets prepared by a solution route at low temperature. These results indicate that Cu doping in the ZnO crystal lattices induces yellow emission because of the oxygen interstitials or the zinc vacancies. The yellow emission shows gradual blue-shifts with the increase of Cu concentrations in the ZnO.[56] However, in our systems, it might arise from the shapes of N-doped ZnO nanowires or the N occupying the ZnO crystal lattices, which were similar to the phosphorus-doped ZnO nanorods by the hydrothermal method.[26] These results are attributed to the P doping in the ZnO crystal lattices. In addition, the N atom is smaller than the P and Cu atoms, thus it causes the visible emission produced by the defect in the crystal of the N-doped ZnO nanowires to have a red-shift.

The refractive dispersion plays an important role in optical materials. In order to calculate the optical constant refractive index (n) and the extinction coefficient (k) of the films at different wavelengths, we applied the following equations:[27,57]

$$\alpha = (1/d)\ln[(1 - R)^2/2T] + (1 - R)^2/(4T^2 + R^2)^{1/2}, \quad (1)$$

$$n = [(R + 1)/(R - 1)] + \{[(R + 1)/(R - 1)]^2 - (1 - k^2)\}^{1/2}, \quad (2)$$

and

$$k = \alpha\lambda/4\pi. \quad (3)$$

In the abovementioned equations, α is the absorption coefficient, d is the film thickness, R is the reflectance, T is the transmittance, and λ is the wavelength. According to the eqn (3), k is related to α and λ. The n and k of PVA, PVA/pristine ZnO (S1) and PVA/N doped ZnO (S2 and S3) hybrid films as a function of the wavelength are shown in Fig. 5a and b, respectively. For the PVA film, the intensity of n remains weak with the increase of the wavelength. The value of n for PVA/S1 film slightly increased along with the wavelength. Comparing it with the hybrid films of PVA/S2 and PVA/S3, we find that in the visible and the near-infrared regions, the value of n increases along with the wavelength. The abovementioned results can also correspond to the measurement of k value. The phenomenon also indicates low light scattering and high absorbance.[27] The increase of the refractive index is attributed to the higher density and the lower

surface roughness of the stacked films with the N-doped ZnO in the PVA matrix (PVA/S2 and PVA/S3)[58] when compared to the refractive index of the PVA/S1 films. We can attribute the result to the decline of volume fraction of the voids on the surface of the PVA hybrid films. This result is different from the Na-doped ZnO thin films[59] and the Cu-doped ZnO films.[60] The results also indicate that the N dopant changes the structural and optical properties of the PVA/N doped ZnO hybrid films. Therefore, we can control the refractive index of the PVA/N doped ZnO hybrid nanocomposite films by varying the composition with the N-doped ZnO nanowire, which is important for the applications in the design of the window products.

The surface and cross-sectional morphologies of the PVA/N doped ZnO hybrid films coated on the glass substrates were investigated by FE-SEM. The PVA/N doped ZnO hybrid films exhibited a homogeneous surface (Fig. 6a), the results are consistent with the n, k results. In addition, the cross-section morphology of the PVA/N doped ZnO hybrid films shows a dense microstructure by stacking between the N-doped ZnO nanowires and PVA matrix, and the thickness of the film is about 300 nm (Fig. 6b). In Fig. 6, we observed that unlike the PVA/N hybrid thin film with ZnO particles, which produce space while they are stacked, the PVA/N doped ZnO hybrid thin film has a rather condensed structure, which can improve the properties of the polymer owing to its even dispersion in the matrix.

4. Conclusions

PVA hybrid thin films with N-doped ZnO nanowires were successfully synthesized by the hydrothermal method in NH$_3$. Measurements of the refractive indices and the extinction

coefficients spectrum showed that the prepared film is capable of insulating a wide-range spectrum for the first time, covering from UV to IR. This wide-range insulating spectrum effect can be attributed to the sharp-sword ZnO nanowires, which are formed by the adsorption of NH_3 on the ZnO crystal lattice. The refractive index of PVA/N doped ZnO hybrid thin films can be controlled by doping various amounts of N in the ZnO nanowires under different NH_3 concentrations. Measurements of the XRD, Raman, and PL spectra proved that the nitrogen was doped into the ZnO wurtzite crystal lattice and substituted for O site to form complex defects. The SEM images also showed that PVA/N doped ZnO hybrid thin films have rather condensed structures and a homogeneous surface. This approach is expected to be a great contribution to enhance the range of insulating wavelength of the PVA hybrid thin film by well-controlling N-doped ZnO nanowires. The result is crucial for the applications of designing effective products of solar heat shielding.

Acknowledgements

References

1 M. Abdullah, T. Morimoto and K. Okuyama, *Adv. Funct. Mater.*, 2003, **13**, 800.

2 N. Dal'Acqua, F. R. Scheffer, R. Boniatti, B. V. M. da Silva, J. V. de Melo, J. da Silva Crespo, M. Giovanela, M. B. Pereira, D. E. Weibel and G. Machado, *J. Phys. Chem. C*, 2013, **117**, 23235.

3 Y. D. Liu, X. Quan, B. Hwang, Y. K. Kwon and H. J. Choi, *Langmuir*, 2014, **30**, 1729.

4 M.-Y. Hua, Y.-C. Lin, R.-Y. Tsai, H.-C. Chen and Y.-C. Liu, *Electrochim. Acta*, 2011, **56**, 9488.

5 L. Y. Ng, A. W. Mohammad, C. P. Leo and N. Hilal, *Desalination*, 2013, **308**, 15.

6 M. Sajimol Augustine, P. P. Jeeju, V. G. Sreevalsa and S. Jayalekshmi, *J. Phys. Chem. Solids*, 2012, **73**, 396.

7 J. Lee, D. Bhattacharyya, A. J. Easteal and J. B. Metson, *Curr. Appl. Phys.*, 2008, **8**, 42.

8 X. M. Sui, C. L. Shao and Y. C. Liu, *Appl. Phys. Lett.*, 2005, **87**, 113115.

9 S. Majumdar and B. Adhikari, *Sens. Actuators, B*, 2006, **114**, 747.

10 Y. Tan, Y. Song and Q. Zheng, *Nanoscale*, 2012, **4**, 6997.

11 H. N. Chandrakala, B. Ramaraj, Shivakumaraiah, J. H. Lee and Siddaramaiah, *J. Alloys Compd.*, 2013, **580**, 392.

12 A. Janotti and C. G. Van de Walle, *Rep. Prog. Phys.*, 2009, **72**, 126501.

13 R. M. Nyffenegger, B. Craft, M. Shaaban, S. Gorer, G. Erley and R. M. Penner, *Chem. Mater.*, 1998, **10**, 1120.

14 L. Irimpan, V. P. N. Nampoori and P. Radhakrishnan, *J. Appl. Phys.*, 2008, **103**, 094914.

15 D. W. Hatchett and M. Josowicz, *Chem. Rev.*, 2008, **108**, 746.

16 S. B. Zhang, S. H. Wei and A. Zunger, *Phys. Rev. B: Condens. Matter Mater. Phys.*, 2001, **63**, 075205.

17 J. Han, F. Fan, C. Xu, S. Lin, M. Wei, X. Duan and Z.-L. Wang, *Nanotechnology*, 2010, **21**, 405203.

18 R. T. Ginting, C. C. Yap, M. Yahaya and M. M. Salleh, *ACS Appl. Mater. Interfaces*, 2014, **6**, 5308.

19 C.-H. Chen, S.-J. Chang, S.-P. Chang, M.-J. Li, I. C. Chen, T.-J. Hsueh, A.-D. Hsu and C.-L. Hsu, *J. Phys. Chem. C*, 2010, **114**, 12422.

20 S.-J. Lim, J.-M. Kim, D. Kim, S. Kwon, J.-S. Park and H. Kim, *J. Electrochem. Soc.*, 2010, **157**, H214.

21 O. Lupan, T. Pauporté, B. Viana, I. M. Tiginyanu, V. V. Ursaki and R. Cortès, *ACS Appl. Mater. Interfaces*, 2010, **2**, 2083.

22 J. A. Anta, E. Guillén and R. Tena-Zaera, *J. Phys. Chem. C*, 2012, **116**, 11413.

23 Y. Xie, P. Joshi, S. B. Darling, Q. Chen, T. Zhang, D. Galipeau and Q. Qiao, *J. Phys. Chem. C*, 2010, **114**, 17880.

24 Y. Zhang, T. R. Nayak, H. Hong and W. Cai, *Curr. Mol. Med.*, 2013, **13**, 1633.

25 B. Sieber, H. Liu, G. Piret, J. Laureyns, P. Roussel, B. Gelloz, S. Szunerits and R. Boukherroub, *J. Phys. Chem. C*, 2009, **113**, 13643.

26 X. Fang, J. Li, D. Zhao, D. Shen, B. Li and X. Wang, *J. Phys. Chem. C*, 2009, **113**, 21208.

27 M. Mazilu, N. Tigau and V. Musat, *Opt. Mater.*, 2012, **34**, 1833.

28 X. Yan, T. Itoh, S. Dai, Y. Ozaki and Y. Fang, *J. Phys. Chem. Solids*, 2013, **74**, 1127.

29 Y. Li, X. Zhao and W. Fan, *J. Phys. Chem. C*, 2011, **115**, 3552.

30 T. P. Rao and M. S. Kumar, *J. Alloys Compd.*, 2010, **506**, 788.

31 P. K. Ooi, S. S. Ng, M. J. Abdullah and Z. Hassan, *Mater. Lett.*, 2014, **116**, 396.

32 H. Wang, R. Bhattacharjee, I. M. Hung, L. Li and R. Zeng, *Electrochim. Acta*, 2013, **111**, 797.

33 C. H. Park, S. B. Zhang and S.-H. Wei, *Phys. Rev. B: Condens. Matter Mater. Phys.*, 2002, **66**, 073202.

34 R. Asahi, T. Morikawa, T. Ohwaki, K. Aoki and Y. Taga, *Science*, 2001, **293**, 269.

35 D. M. Fernandes, A. A. W. Hechenleitner, S. M. Lima, L. H. C. Andrade, A. R. L. Caires and E. A. G. Pineda, *Mater. Chem. Phys.*, 2011, **128**, 371.

36 S. Tan, X. Tan, J. Jiang, J. Xu, J. Zhang, D. Zhao, L. Liu and Z. Huang, *J. Electroanal. Chem.*, 2012, **668**, 113.

37 A. S. Roy, S. Gupta, S. Sindhu, A. Parveen and P. C. Ramamurthy, *Composites, Part B*, 2013, **47**, 314.

38 H. Qin, W. Li, Y. Xia and T. He, *ACS Appl. Mater. Interfaces*, 2011, **3**, 3152.

39 D. G. Cahen, J. -Marc, C. Schmitz, L. Chernyak, K. Gartsman and A. Jakubowicz, *Science*, 1992, **258**, 271.

40 L. Duan, W. Zhang, X. Yu, P. Wang, Z. Jiang, L. Luan, Y. Chen and D. Li, *Solid State Commun.*, 2013, **157**, 45.

41 W.-W. Zhong, F.-M. Liu, L.-G. Cai, X.-Q. Liu and Y. Li, *Appl. Surf. Sci.*, 2011, **257**, 9318.

42 K. A. Alim, V. A. Fonoberov and A. A. Balandin, *Appl. Phys. Lett.*, 2005, **86**, 053103.

43 B. M. Keyes, L. M. Gedvilas, X. Li and T. J. Coutts, *J. Cryst. Growth*, 2005, **281**, 297.

44 N. P. Herring, L. S. Panchakarla and M. S. El-Shall, *Langmuir*, 2014, **30**, 2230.

45 Z. W. Dong, C. F. Zhang, H. Deng, G. J. You and S. X. Qian, *Mater. Chem. Phys.*, 2006, **99**, 160.

46 J. Karamdel, C. F. Dee and B. Y. Majlis, *Appl. Surf. Sci.*, 2010, **256**, 6164.

47 A. Kaschner, U. Haboeck, M. Strassburg, M. Strassburg, G. Kaczmarczyk, A. Hoffmann, C. Thomsen, A. Zeuner, H. R. Alves, D. M. Hofmann and B. K. Meyer, *Appl. Phys. Lett.*, 2002, **80**, 1909.

48 S. Dhara and P. K. Giri, *Thin Solid Films*, 2012, **520**, 5000.

49 L.-C. Chao, J.-W. Chen, H.-C. Peng and C.-H. Ho, *Surf. Coat. Technol.*, 2013, **231**, 492.

50 P. K. Samanta and P. R. Chaudhuri, *Sci. Adv. Mater.*, 2011, **3**, 107.

51 A. Umar, B. Karunagaran, E. Suh and Y. Hahn, *Nanotechnology*, 2006, **17**, 4072.

52 J.-F. Chien, C.-H. Chen, J.-J. Shyue and M.-J. Chen, *ACS Appl. Mater. Interfaces*, 2012, **4**, 3471.

53 D. Y. Lee, J.-E. Cho, N.-I. Cho, M.-H. Lee, S.-J. Lee and B.-Y. Kim, *Thin Solid Films*, 2008, **517**, 1262.

54 J. W. Chiou, K. P. K. Kumar, J. C. Jan, H. M. Tsai, C. W. Bao, W. F. Pong, F. Z. Chien, M.-H. Tsai, I.-H. Hong, R. Klauser, J. F. Lee, J. J. Wu and S. C. Liu, *Appl. Phys. Lett.*, 2004, **85**, 3220.

55 Q. Zhao, X. Y. Xu, X. F. Song, X. Z. Zhang, D. P. Yu, C. P. Li and L. Guo, *Appl. Phys. Lett.*, 2006, **88**, 033102.

56 R.-C. Wang and H.-Y. Lin, *Mater. Chem. Phys.*, 2011, **125**, 263.

57 S. Ilican, M. Zor, Y. Caglar and M. Caglar, *Opt. Appl.*, 2006, **36**, 29.

58 Y. Okuhara, T. Kato, H. Matsubara, N. Isu and M. Takata, *Thin Solid Films*, 2011, **519**, 2280.

59 J. Lv, K. Huang, X. Chen, J. Zhu, C. Cao, X. Song and Z. Sun, *Opt. Commun.*, 2011, **284**, 2905.

60 M. Caglar and F. Yakuphanoglu, *Appl. Surf. Sci.*, 2012, **258**, 3039.